Electronic Supplementary Material (ESI) for Energy & Environmental Science.

Supporting Information

Production of drop-in fuel from biomass at high selectivity by combined microbial and electrochemical conversion

Carolin Urban[a], Jiajie Xu[b], Heike Sträuber[a], Tatiane R. dos Santos Dantas[a], Jana Mühlenberg[c], Claus Härtig[a], Largus T. Angenent[b, d], Falk Harnisch[a]*

[a] UFZ – Helmholtz-Centre for Environmental Research; Department of Environmental Microbiology; Permoserstraße 15, 04318 Leipzig (Germany); fax: (+49) 341 235 – 1351; E-mail: falk.harnisch@ufz.de

[b] Cornell University; Department of Biological and Environmental Engineering, 226 Riley–Robb Hall, Ithaca, NY 14853 (USA)

[c] DBFZ – Deutsches Biomasseforschungszentrum gemeinnützige GmbH; Department Biochemical Conversion, Torgauer Straße 116, 04347 Leipzig (Germany)

[d] University of Tübingen; Center for Applied Geoscience, Hölderlinstr. 12, 72074 Tübingen (Germany)

*author of correspondence: falk.harnisch@ufz.de

Table of content

S 1 Theoretical background and calculations

Table S 1: List of abbreviations and symbol directory.

Abbreviation/ Symbol	Name	Unit
$A_{electrode}$	geometrical surface area of the working electrode	cm^2
ASBR	anaerobic sequencing batch bioreactor (case study A)	-
B_1 - B_4	factors for temperature dependent density conversion	-
bp	boiling point	°C
c_i	concentration of CA with *i* C-atoms (*i* = 3..8)	mol L^{-1}
$c_{i\_b\_tx}$	concentration of CA with *i* C-atoms (*i* = 3..8) in the back-extraction solution of case study A at time t_x with *x* = 0 or 1	g L^{-1}
$c_{i\_e\_tx}$	concentration of CA with *i* C-atoms (*i* = 3.8) in the effluent of case study A at time t_x with *x* = 0 or 1	g L^{-1}
C_i	*n*-carboxylic acid with *i* C-atoms (*i* = 3..8)	-
$c(A^-)$	concentration of dissociated CA	mol L^{-1}
c(HA)	concentration of protonated CA	mol L^{-1}
CA	carboxylic acid	-
CE	coulombic efficiency	%
CH_4	methane	-
CN	cetane number	-
CO_2	carbon dioxide	-
COD	chemical oxygen demand	g g^{-1}
E_{CE}	counter electrode potential, expressed *vs.* Ag/AgCl sat.	V
E_{cell}	cell potential	V
E_{WE}	working electrode potential, expressed *vs.* Ag/AgCl sat.	V
F	Faraday constant, 96485.33 C mol^{-1}	C mol^{-1}
f_{COD_Ci}	conversion factor – gravimetric COD content per mass equivalent of C_i	g COD g^{-1}
FAME	fatty acid methyl esters	-
FE	Farad equivalents	-
$feed_{cornbeer}$	daily substrate feed of corn beer in case study A	g COD L d^{-1}
GC-MS	gas chromatography-mass spectrometry	-

Continuation Table S1. List of abbreviations and symbol directory.

Abbreviation/ Symbol	Name	Unit
GC-TCD	gas chromatography-thermal conductivity detector	-
H_2	hydrogen	-
HRT	hydraulic retention time of substrate in case study A	d
HPLC	high performance liquid chromatography	-
HVO	hydrogenated vegetable oil	-
i	current	A
IS	inert solids	-
j_{av}	aveage area-related current density	mA cm^{-2}
j_{max}	maximum area-related current density	mA cm^{-2}
m_{Ci_tj}	the total gravimetric CA content in the process liquid at time t_j with j = 0 or 1	kg
m_{COD_Ci}	COD content per mol of C_i	g COD mol^{-1}
M_i	molar mass of component i = C_i or O_2	g mol^{-1}
MCCA	medium-chain carboxylic acids (six to twelve carbon atoms)	-
N_2	nitrogen	-
n_{CA_elec}	amount of electrochemically converted CA	mol
n_{CA_tot}	total amount of CA in electrolysis volume	mol
n_{O2_Ci}	amount of oxygen demand per complete oxidation of C_i	mol O_2 mol^{-1}
opex	operating expenditures	€ / US$
p_0	normal pressure, 101325 Pa	Pa
p_L	ambient air pressure	Pa
p_W	vapor pressure of water in dependency of the ambient temperature	Pa
P_{WE}	power input for the electrochemical half cell reaction at the working electrode	W
Q_{CA_elec}	charge that is theoretically required to convert the electrochemically converted educt molecules in solution (n_{CA_elec})	C
Q_{CA_tot}	charge that is theoretically required to convert *all* educt molecules in solution (n_{CA_tot})	C
Q_t	charge that was transferred during electrolysis	C

Continuation Table S1. List of abbreviations and symbol directory.

Abbreviation/ Symbol	Name	Unit
$r_{Ci\_d\_k}$	daily CA production rate of CA with *i* C-atoms for case study *k* = A or B	g L^{-1} d^{-1}
r_{CA}	electrochemical CA conversion rate	mol cm^{-2} h^{-1}
t	time	s
T	ambient temperature	K
T_0	normal temperature, 273 K	K
t_{elec}	duration of the electrolysis	h
TS	total solids	% (fresh mass)
V_0	normal volume	m^3
V_{ASBR}	working volume anaerobic bioreactor in case study A	L
$V_{effluent}$	liquid volume of the effluent exchanged in the semi-continuous operation of bioreactor operated in case study A (exchange of 666 mL every 48 h)	L
$V_{extraction}$	liquid volume of the alkaline back-extraction solution in case study A	L
$V_{gas\_measured}$	gas volume estimated via water displacement	m^3
$V_{leach\text{-}bed\ reactor}$	working volume of the leach-bed reactor in case study B	L
VS	volatile solids	% (TS)
W_{WE}	energy input to the electrochemical half cell reaction per converted mol of CA	kWh mol^{-1}
z	charge transfer number	-
Greek letters		
ρ	density	g cm^{-3}
κ	electrolytic conductivity	mS cm^{-1}

S 1.1 Accessing the share of dissociated carboxylic acid molecules

The share of dissociated CA molecules in aqueous solution in dependency of the solution pH was estimated applying the Henderson-Hasselbalch-equation (eq. S1), with $c(A^-)$ being the concentration of CA ions and $c(HA)$ being the protonated form of the CA. Further, it is known that the sum of $c(A^-)$ and $c(HA)$ equals the total concentration of CA in solution (with i C-atoms), c_i, (eq. S2). Consequently, eq. S1 and eq. S2 can be joined to give eq. S3 which gives the concentration of dissociated CA molecules in dependence of the pH. Relating $c(A^-)$ to c_{CA} equals the share of dissociated CA molecules.

$$pH = pK_a + log_{10}\left(\frac{c(A^-)}{c(HA)}\right) \quad \text{(eq. S1)}$$

$$c_i = c(A^-) + c(HA) \quad \text{(eq. S2)}$$

$$c(A^-) = \frac{c_i \cdot 10^{(pH - pK_a)}}{1 + 10^{(pH - pK_a)}} \quad \text{(eq. S3)}$$

S 1.2 Evaluation of the microbial carboxylic acid production

S 1.2.1 Step 1 – *Bioreactor*: Carboxylic acid production rate

In case study A, the daily production rate of the carboxylic acids (CA) containing i C-atoms, $r_{Ci\_d\_A}$, was determined according to eq. S4 considering: (*i*) the gravimetric amount of CA that was removed from the bioreactor via the effluent stream (*i.e.* the gravimetric CA concentration in the effluent at the time t_1, $c_{i\_e\_t1}$) times the effluent volume, $V_{effluent}$ (666 mL every 48 h, cf. experimental section), in relation to the hydraulic retention time, HRT, of 15 d; as well as (*ii*) the CA accumulating in the alkaline back-extraction solution (*i.e.* the delta in the gravimetric CA concentration in the back-extraction solution, $c_{i\_b\_t1} - c_{i\_b\_t0}$) times the liquid volume of the back-extraction solution, $V_{extraction}$, related to the delta in operating time, $t_1 - t_0$. The total amount of accumulating CA from (*i*) and (*ii*) (expressed in g d^{-1}) was summed up and related to the liquid bioreactor volume, V_{ASBR} (= 5 L). Table S2 lists a *representative production rate* for CA (medium- and short-chain) for the described bioreactor conditions.

$$r_{Ci\_d\_A} = \left[\frac{c_{i\_e\_t1} \cdot V_{ASBR}}{HRT} + \frac{(c_{i\_b\_t1} - c_{i\_b\_t0})V_{extraction}}{(t_1 - t_0)}\right] \cdot \frac{1}{V_{ASBR}} \quad \text{(eq. S4)}$$

In case study B, the maximum production rate of CA in the batch setup was accessed by eq. S5, where $r_{Ci\_d\_B}$ is the maximum production rate of C_i in case study B (in g_{Ci} L^{-1} d^{-1}), m_{Ci_t1} and m_{Ci_t0} are the total CA amounts in the process liquid (in g) at the operating times t_1 and t_0, respectively, $V_{leach\text{-}bed\ reactor}$ is the working volume of the leach-bed reactor (= 11.5 L) and t_0 and t_1 are beginning and end of the maximum production period of CA (in d), respectively.

$$r_{Ci\_d\_B} = \frac{m_{Ci\_t1} - m_{Ci\_t0}}{(t_1 - t_0) \cdot V_{leach-bed\,reactor}} \qquad \text{(eq. S5)}$$

S 1.2.2 Chemical oxygen demand and carboxylic acid yield

To determine the chemical oxygen demand (COD), per CA, *i.e.* the amount of oxygen required for a complete oxidation of the particular CA to carbon dioxide and water, the chemical equation needs to be accessed and the amount of oxygen in mol per mol CA, n_{O2_Ci}, needs to be determined (step 1). Then, n_{O2_C}, times the molar mass of oxygen, M_{O2}, equals the COD of one mol equivalent of the specific CA, m_{COD_Ci} (step 2). Relating m_{COD_Ci} to the molar mass of the CA, M_{Ci}, equals the conversion factor, f_{COD_Ci}, between one mass equivalent of the CA to one mass equivalent of COD (step 3). The yield of the individual CA with *i* C-atoms, C_i, produced (in g) per fed substrate in the case studies A and B was calculated in respect to the volumetric or gravimetric unit of the substrate (step 4). Similarly, the CA yield can be expressed in COD equivalents per COD equivalent of the substrates (step 5).

Step 1: Complete oxidation of *n*-caproic acid, *n*-caprylic acid and *n*-butyric acid.

$$C_6H_{12}O_2 + 8\,O_2 \rightarrow 6\,CO_2 + 6\,H_2O \qquad \left(n_{O2\_C6} := 8\frac{mol_{O2}}{mol_{C6}}\right)$$

$$C_8H_{16}O_2 + 11\,O_2 \rightarrow 8\,CO_2 + 8\,H_2O \qquad \left(n_{O2\_C8} := 11\frac{mol_{O2}}{mol_{C8}}\right)$$

$$C_4H_8O_2 + 5\,O_2 \rightarrow 4\,CO_2 + 4\,H_2O \qquad \left(n_{O2\_C4} := 5\frac{mol_{O2}}{mol_{C4}}\right)$$

Step 2: Chemical oxygen demand (COD) for oxidation of one mol *n*-caproic acid (*n*-caprylic acid and *n*-butyric acid).

$$n_{O2\_Ci} \cdot M_{O2} = m_{COD\_Ci}$$

$$8\frac{mol_{O2}}{mol_{C6}} \cdot 32\frac{g_{O2}}{mol_{O2}} = 256\frac{g_{COD}}{mol_{C6}}$$

$$\left(11\frac{mol_{O2}}{mol_{C8}} \cdot 32\frac{g_{O2}}{mol_{O2}} = 352\frac{g_{COD}}{mol_{C8}} \quad and \quad 5\frac{mol_{O2}}{mol_{C4}} \cdot 32\frac{g_{O2}}{mol_{O2}} = 160\frac{g_{COD}}{mol_{C4}}\right)$$

Step 3: Mass equivalent COD to *n*-caproic acid (*n*-caprylic acid and *n*-butyric acid) conversion factor using the respective molar masses, *e.g.*, $M_{C6} = 116.16\frac{g_{C6}}{mol_{C6}}$

$$f_{COD\_C6} = \frac{256\frac{g_{COD}}{mol_{C6}}}{116.16\frac{g_{C6}}{mol_{C6}}} \approx 2.204\frac{g_{COD}}{g_{C6}}$$

$$\left(f_{COD\_C8} = \frac{352\frac{g_{COD}}{mol_{C8}}}{144.21\frac{g_{C8}}{mol_{C8}}} \approx 2.441\frac{g_{COD}}{g_{C8}} \quad and \quad f_{COD\_C4} = \frac{160\frac{g_{COD}}{mol_{C4}}}{88.11\frac{g_{C4}}{mol_{C4}}} \approx 1.816\frac{g_{COD}}{g_{C4}}\right)$$

Step 4 – case study A: CA yield per volumetric substrate unit (L) in case study A is calculated as follows: Every 48 h, 666 mL of the 5 L bioreactor volume, V_{ASBR}, were exchanged with diluted fresh substrate. From the total feed of 666 mL, 166 mL were corn beer so that 166 mL fresh corn beer was fed every 48 h per 5 L. This equals a feed of $feed_{cornbeer}$ = 0.0166 L_{corn_beer} L^{-1} d^{-1}. The absolute yield of CA per corn beer can calculated as follows:

$$absolute\ CA_i\ yield\ per\ substrate = \frac{r_{Ci\_d\_A}}{feed_{corn\ beer}}$$

Step 4 – case study B: CA yield per fed gravimetric substrate unit of dry substrate in case study B

$$absolute\ CA_i\ yield\ per\ substrate = \frac{end\ concentration\ of\ CA\left[\frac{g}{L}\right] \cdot V_{leach-bed\ reactor}}{total\ fresh\ mass\ of\ corn\ silage\ per\ batch}$$

Step 5 – case study A: The absolute CA yield per substrate is converted into a yield of COD equivalents per COD of corn beer in case study A (COD content of corn beer, see Table S5):

$$COD\ eqivalent\ CA_i\ yield = \frac{absolute\ CA_i\ yield\ per\ substrate \cdot f_{COD\_Ci}}{0.460 \frac{g_{COD}}{L_{substrate}}}$$

Step 5 – case study B: The absolute CA yield per substrate is converted into a yield of COD equivalents per COD of corn silage in case study B (COD content of corn silage, see Table S6):

$$COD\ eqivalent\ CA_i\ yield = \frac{absolute\ CA_i\ yield\ per\ substrate \cdot f_{COD\_Ci}}{0.337 \frac{g_{COD}}{g_{substrate}}}$$

S 1.2.3 Step 2 – *Pertraction*: Minimum extraction time to recover 1 mol L^{-1} carboxylic acid in back-extraction solution

One critical parameter is the duration of microbial CA production in relation to the duration of the CA electrolysis, *i.e.* the extraction time that is required to achieve a certain target concentration of CA prior to electrolysis. Here we have assumed 1 mol L^{-1} as threshold. For an optimized extraction system, it is assumed that 95% extraction efficiency is achieved for MCCA[1]. Further, the volume ratio of bioreactor liquid to back-extraction solution equals 10:1 in the assumed optimized extraction system.

We now adopt the assumptions for an optimized extraction in the case study A, yielding mainly easily extractable MCCA. For *n*-caproic acid, 1.743 g COD L^{-1} d^{-1} was produced in the bioreactor. When multiplying this rate by 95% extraction efficiency and by the volume ratio 10 L L^{-1} (bioreactor to extraction solution), 16.56 g COD L^{-1} (extraction solution) d^{-1} *n*-caproic

acid would daily accumulate in the back-extraction solution (6.5×10^{-2} mol L^{-1} d^{-1}). Additionally, 2.695 g COD L^{-1} (bioreactor) d^{-1} *n*-caprylic acid times 95% extraction efficiency times 10 L L^{-1} (bioreactor to extraction solution) equals 25.6 g COD L^{-1} *n*-caprylic acid accumulation rate in the back-extraction solution (7.3×10^{-2} mol L^{-1} d^{-1}). When now relating the sum of the daily accumulating MCCA to the target concentration of CA in the back-extraction solution (1 mol L^{-1}), the minimum extraction time would be shortened to ≈7.3 d assuming optimized extraction, but identical fermentation performance as observed in case study A.

S 1.3 Step 3 – *Kolbe electrolysis*: Electrolysis performance

For better comparability, all electrolysis were set to achieve ≈0.6 Farad equivalents (FE). In this study, FE (eq. S6) are defined as the ratio between the charge that is transferred over time, Q_t (eq. S7), and the charge that is theoretically required to convert all educt molecules in solution (*i.e.* CA molecules), Q_{CA_tot}. Q_{CA_tot} is calculated according to Faraday's law (eq. S8), with *F* being the Faraday constant, *z* being the charge transfer number (*i.e.* the number of electrons transferred per oxidation or reduction of the target compound, here: $z = 1$ since hydrocarbon products of the electrolysis are preferred, cf. Figure S1) and n_{CA_tot} being the amount of CA molecules in the reaction volume (*i.e.*, CA concentration in mol L^{-1} times reaction volume in L). The Coulombic efficiency (*CE*, eq. S9) is assumed to equal 100% for determining the charge to be transferred during each electrolysis to achieve ≈0.6 FE (Q_t = 2800 C).

$$FE\,(t) = \frac{Q_t}{Q_{CA\_tot}} = \frac{\int_0^t idt}{n_{CA\_tot} \cdot F \cdot z} \qquad \text{(eq. S6)}$$

$$Q_t(t_{elec}) = \int_0^{t_{elec}} idt \qquad \text{(eq. S7)}$$

$$Q_{CA\_i} = n_{CA\_i} \cdot F \cdot z \quad i = tot \;\; OR \;\; i = elec \qquad \text{(eq. S8)}$$

The *CE* was defined as the ratio between Q_t and the charge that is theoretically required to convert the amount of CA molecules that were oxidized during the electrolysis, Q_{CA_elec} and n_{CA_elec}, based on the difference in CA concentration before and after electrolysis as accessed via HPLC analysis assuming $z = 1$ (eq. S9).

Throughout the electrolysis experiments, the working electrode potential, E_{WE}, was set to +3 V *vs.* Ag/AgCl (sat. KCl) and the counter electrode potential, E_{CE}, was varying. The difference between E_{WE} and E_{CE} is the cell potential, E_{cell}. The power input for the electrochemical half cell reaction at the working electrode, P_{WE}, is defined as the product of current, i, and E_{WE} (eq. S10) and was accessed as described earlier[2]. The maximum current density, j_{max}, was calculated by dividing the maximum current read out of the current-time curve by geometrical surface area of the working electrode, $A_{electrode}$.

$$CE = \frac{Q_{CA\_elec}}{Q_t} \qquad \text{(eq. S9)}$$

$$P_{WE} = i \cdot E_{WE} \qquad \text{(eq. S10)}$$

The electric energy for the half cell reaction to convert 1 mol of CA, W_{WE}, was calculated using eq. S11, by relating the electric energy consumed during the electrolysis to convert the amount of CA that was actually converted (accessed by HPLC sampling, see below), n_{CA_elec}.

$$W_{WE} = \frac{P_{WE} \cdot t_{elec}}{n_{CA\_elec}} \qquad \text{(eq. S11)}$$

The rate of electrochemical CA conversion, r_{CA}, was calculated according to eq. S12, by relating n_{CA_elec} to t_{elec} and the geometrical electrode surface area, $A_{electrode}$, of the working electrode.

$$r_{CA} = \frac{n_{CA\_elec}}{t_{elec} \cdot A_{electrode}} \qquad \text{(eq. S12)}$$

Finally, the carbon balance of the electrolysis step was evaluated. For this, the total amount of C-atoms bound in the electrolysis products was related to the amount of C-atoms in the CA that were electrochemically converted. The total amount of C-atoms recovered in the identified electrolysis products was accessed by multiplying the molar concentration of each compound by its number of C-atoms and the electrolysis volume (50 mL) and summing up over all identified products (except CO_2), *e.g.* 1 mol *n*-tetradecane contains 14 mol C-atoms, assuming a *n*-tetradecane concentration of 1×10^{-2} mol L^{-1} *n*-tetradecane in 0.05 L, this equals 7×10^{-3} mol of the C-atoms recovered in the electrolysis product. The consumed C-atoms during CA oxidation were similarly assessed. First, the molar CA consumption was derived from HPLC or GC-MS data (section 3.2). For each individual CA with *i* C-atoms, the delta in molar CA concentration was multiplied by the electrolysis volume. Due to the

decarboxylation step (Figure S1), the delta in CA molecules was multiplied by *i*-1 to yield the amount of C-atoms recoverable in the electrolysis product per CA, which was then summed up over all CA. This approach for the carbon balance is valid for each potential electrolysis product except for esters, where one of the two CA still contains the CO_2. However, esters were only found in minor quantities.

S 1.4 Process scheme for carboxylic acid electrolysis (oxidation)

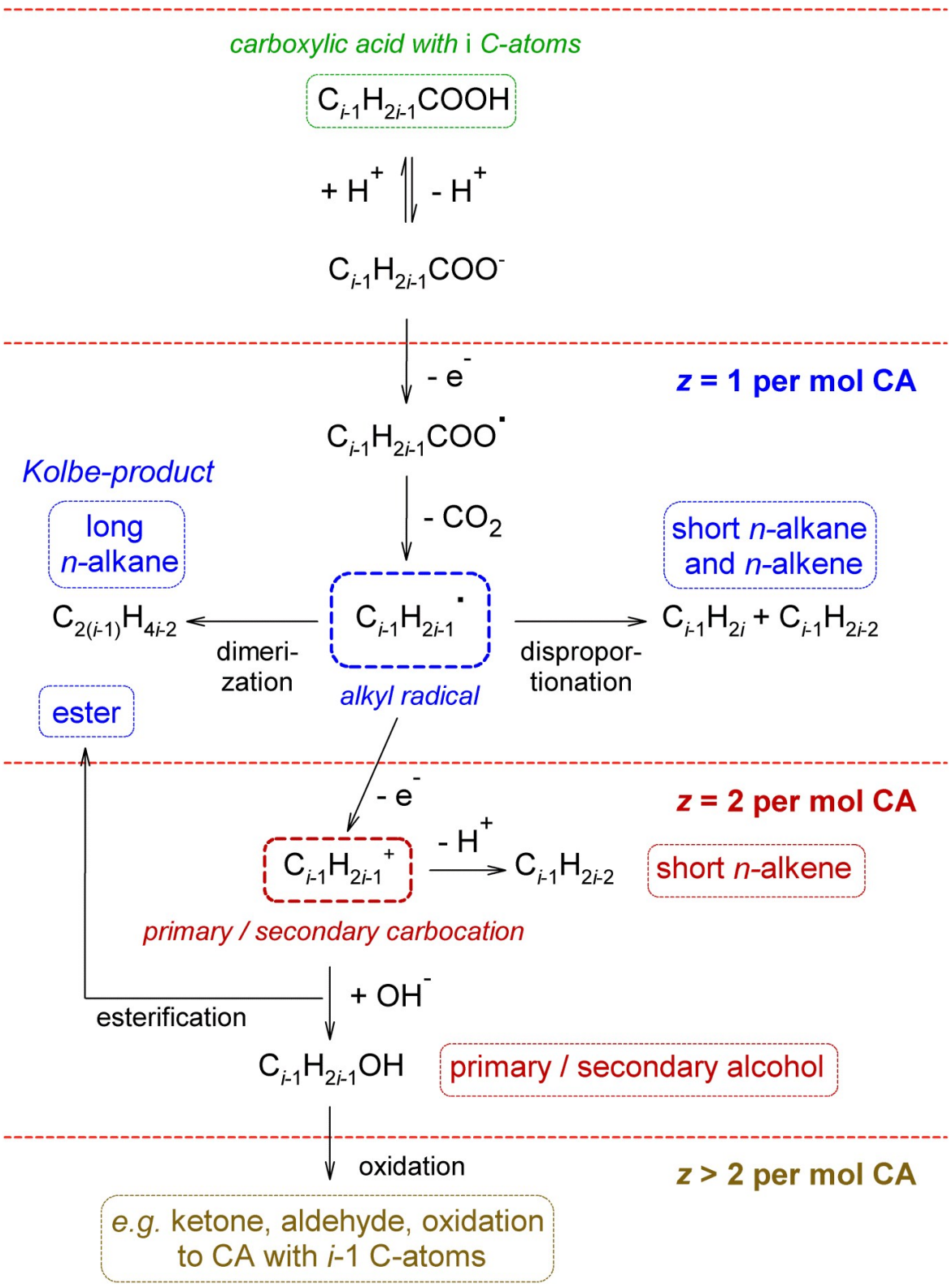

Figure S 1: Reaction pathways for CA electrolysis adapted from[3]: The carboxylate ion with *i* C-atoms can be oxidized at positive potentials (>2.5 V *vs.* standard hydrogen electrode) to yield a reactive alkyl radical (z = 1). The alkyl radical undergoes follow-up reactions yielding different electrolysis products, for example the Kolbe-product is derived from the dimerization of two alkyl radicals. In case the alkyl radical is oxidized to a carbocation, the derived products are considered z = 2 products.

S 2 Results

S 2.1 Details on the performance of the microbial and electrochemical conversions

S 2.1.1 Step 1 (*Bioreactor*) and step 3 (*Kolbe electrolysis*) - Production rates and yields of carboxylic acids and hydrocarbons

Table S 2: Summary of Step 1 – *Bioreactor:* The representative (case study A) or maximum (case study B) CA production rates during anaerobic fermentation. Calculations are presented in eq. S4-S5; step 1-4.

Parameter	**Case study A** (corn beer)	**Case study B** (corn silage)
COD content of substrate	460 g COD L^{-1}	337 g COD kg^{-1}
volumetric loading rate of bioreactor	7.64 g COD L^{-1} d^{-1}	117.4 g COD L^{-1} (13 d batch)
fraction of fed COD that was degraded	63.4%	45.6%
volumetric production rate of CA	**[g L^{-1} h^{-1}]**	**[g L^{-1} h^{-1}]**
propionic acid	*	0.009
n-butyric acid	0.008	0.166
n-valeric acid	*	0.001
n-caproic acid	0.033	0.013
n-enanthic acid	0.001	0.000
n-caprylic acid	0.046	0.001
iso-CA	0.001	0.005
volumetric production rate of CA	**[g COD L^{-1} d^{-1}]**	**[g COD L^{-1} d^{-1}]**
propionic acid	0.008	0.141
n-butyric acid	0.330	2.187
n-valeric acid	0.010	0.016
n-caproic acid	1.743	0.144
n-enanthic acid	0.056	0.001
n-caprylic acid	2.695	0.005
iso-CA	0.030	0.065
sum C_4, C_6, C_8	4.778	n.a.**
sum *n*- and *iso*-MCCA	4.496	n.a.**
sum total CA ≥3 C-atoms	4.872	n.a.**

* traces, below limit of detection. ** summing up volumetric production rates of CA is not applicable for case study B, as CA are produced consecutively during batch mode (Figure S2).

Table S 3: Summary of Step 1 – *Bioreactor* and Step 3 – *Kolbe electrolysis*: Representative (case study A) and maximum achieved (case study B) yields for anaerobic CA production and electrolysis of CA enriched back-extraction solution in case studies A and B, respectively.

Parameter	**Case study A** (corn beer, composition in Table S5)	**Case study B** (corn silage, composition in Table S6)
Yield of product per substrate (COD) added to the *bioreactor*	**[g COD g^{-1} COD]**	**[g COD g^{-1} COD]**
	Step 1 - *Bioreactor*	
propionic acid	0.001	0.018
n-butyric acid	0.043	0.207
n-valeric acid	0.001	0.004
n-caproic acid	0.228	0.030
n-enanthic acid	0.007	0.000
n-caprylic acid	0.353	0.001
iso-CA	0.004	0.016
sum C_4, C_6, C_8	0.626	0.238
sum *n*- and *iso*-MCCA	0.589	0.038
sum total CA ≥3 C-atoms	0.638	0.276
	Step 3 - *Kolbe electrolysis*	
hydrocarbon	0.480	0.085
total organic product	0.499	0.126
Yield of product per substrate (fresh mass) added to the *bioreactor*	**[g L^{-1}]**	**[g kg^{-1}]**
	Step 1 - *Bioreactor*	
propionic acid	0.3	4.0
n-butyric acid	11.0	38.4
n-valeric acid	0.3	0.7
n-caproic acid	47.7	4.5
n-enanthic acid	1.4	0.03
n-caprylic acid	66.5	0.2
iso-CA	0.9	2.8
sum C_4, C_6, C_8	125.1	43.1
sum *n*- and *iso*-MCCA	115.7	5.9
sum total CA ≥3 C-atoms	128.1	50.7
	Step 3 - *Kolbe electrolysis*	
hydrocarbon	63.7	8.3
total organic product	67.2	15.6

S 2.1.2 Step 1 – *Bioreactor*: Carboxylic acid fermentation off-gas

Apart from CA, also biogas is produced during the CA fermentation in case study A and case study B, containing energy rich CH_4 and H_2 that can both be used energetically on-site. In case study A, the fermentation off-gas consisted of mainly CH_4 (54 $\pm$ 14%) and nitrogen (N_2, 41 $\pm$ 12%), but also contained minor amounts of CO_2 (1.2 $\pm$ 0.8%) and H_2 (0.4 $\pm$ 0.2%). On average, a highly fluctuating daily biogas production of 0.034 $\pm$ 0.026 L L^{-1} d^{-1} [gas/ bioreactor volume] was recorded in case study A. For example, about 0.018 L L^{-1} d^{-1} CH_4 were produced daily, which is equivalent to 0.002 L g^{-1} COD [CH_4 / substrate COD].

The composition of the fermentation gas in case study B was highly fluctuating due to the different sequential processes occurring during batch processing, containing CH_4 (2.9 $\pm$ 3.5%), N_2 (36.7 $\pm$ 15.8%), CO_2 (48.3 $\pm$ 20.0%) and H_2 (3.9 $\pm$ 6.5%). No quantitative data for the gas volume flow is available for case study B.

S 2.2 Step 1 – *Bioreactor:* Carboxylic acid production in case study B (batch)

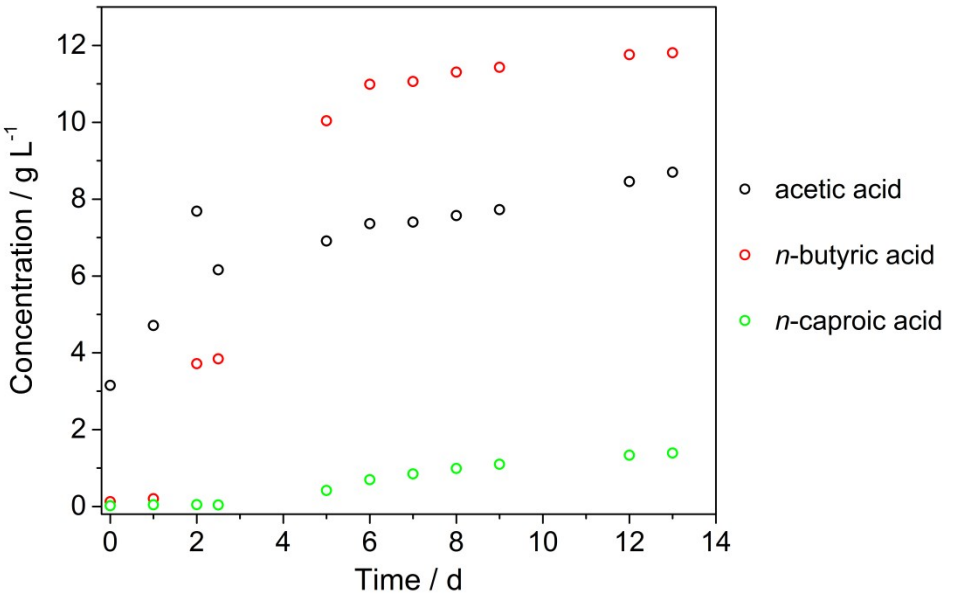

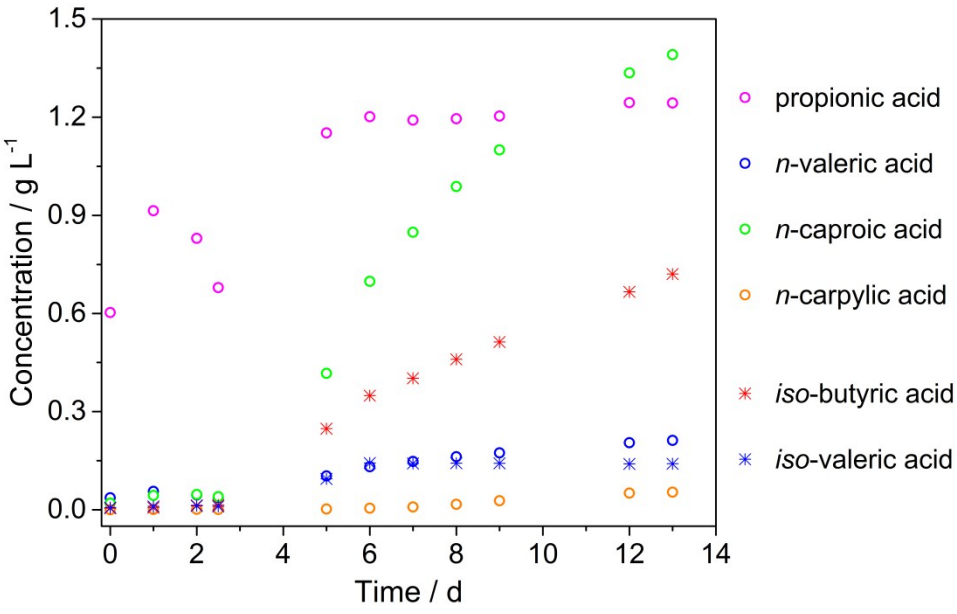

Figure S 2: Carboxylic acid production from corn silage in case study B over time, with initially preferred acetic and *n*-butyric acid accumulation followed by *n*-caproic acid accumulation.

S 2.3 Step 3 – *Kolbe electrolysis:* Liquid, non-aqueous carboxylic acid electrolysis product composition

Figure S3 shows the phase separation of the non-aqueous and the aqueous phase after electrolyzing 100 mL of the exemplary CA mixture for accessing the fuel characteristics of the non-aqueous electrolysis product.

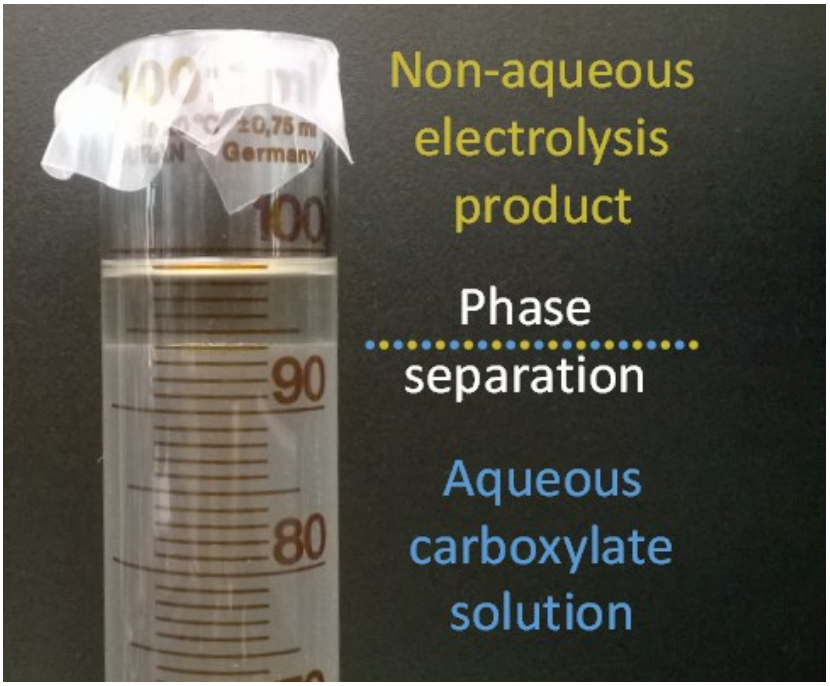

Figure S 3: Photograph of phase separation of the aqueous phase and the non-aqueous liquid product phase after electrolysis.

The exemplary solution mirroring the CA composition of the back-extraction solution of case study A had a higher pH (12.0) and thus, a slightly higher conductivity (34.8 mS cm^{-1}). However, this did not result in major differences in electrolysis performance and the liquid electrolysis product composition, *i.e.* the product spectrum derived from the exemplary CA mixture was almost identical to the observations in case study A (Figure S4). In short, *n*-alkanes in the range of *n*-heptane to *n*-tetradecane (and traces of *n*-pentadecane) were the main components (85.5%) followed by *n*-alkenes, covering 9.6% based on the mol fraction. Further components were esters (2.3%), alcohols (0.5%), octanoic acid (0.3%) and others. This similarity in composition justifies that the parameters for the evaluation of the applicability of the electrolysis product as drop-in biofuel were derived from electrolysis experiments using the exemplary CA mixture.

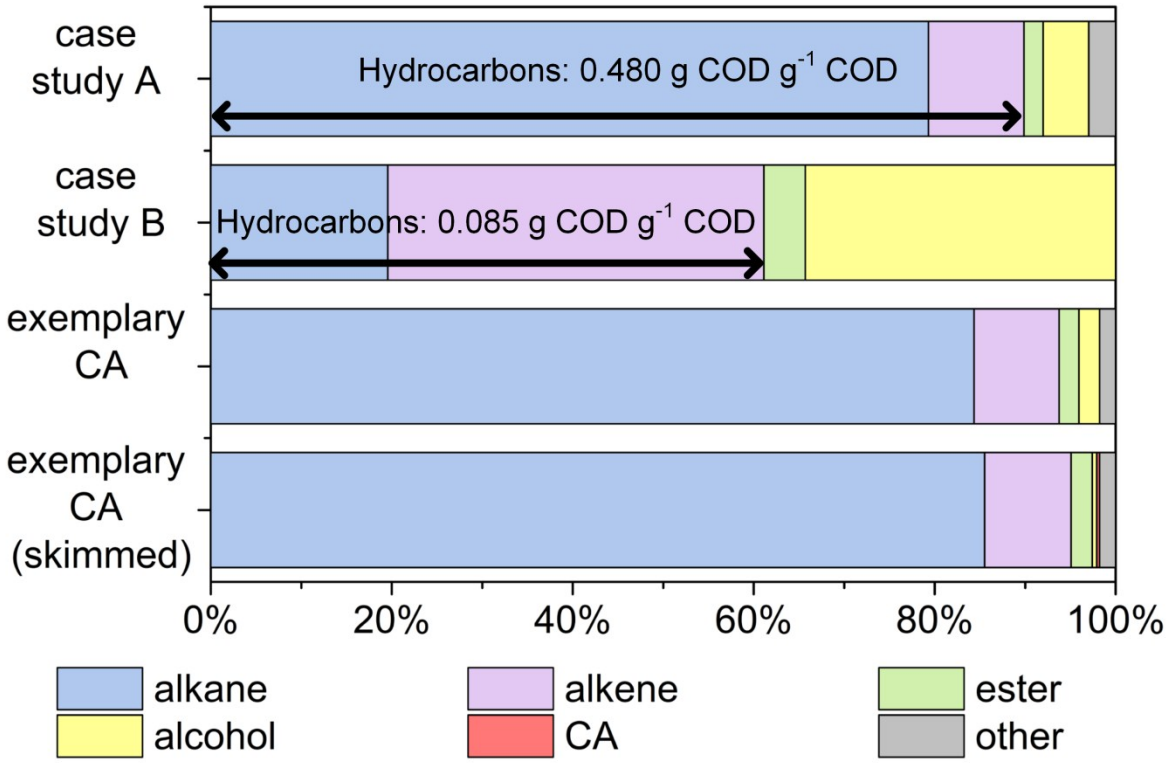

253

254 **Figure S 4:** Composition of the liquid electrolysis product of the exemplary CA mixture in comparison
255 to case study A and case study B. From top to bottom: case study A or B electrolysis product
256 composition after extracting the total aqueous volume in *n*-pentane, pure non-aqueous phase
257 skimmed off the exemplary CA sample (without *n*-pentane extraction step); exemplary CA electrolysis
258 product composition after extracting the total aqueous volume in *n*-pentane. The illustrated
259 hydrocarbon yield relates to the COD of the subtrate fed to the bioreactor (corn beer or corn silage for
260 case studies A or B, respectively).

261

262 The most prominent difference in composition of the electrolysis products concerns the
263 amount of alcohols, which was lower for the collected non-aqueous electrolysis product
264 phase for the exemplary CA solution compared to the electrolysis results in case study A
265 (0.7% *vs.* 5.2% alcohol content, Figure S4). This observation could partly be explained by the
266 different analysis protocols (cf. section S. 3.2.2 experimental section). As alcohols are slightly
267 more soluble in water than the *n*-alkanes, especially when considering that the majority of the
268 *n*-alkanes possess a longer carbon chain (C_7 to C_{14}) than the detected alcohols (C_5 to C_7), it
269 is possible that the alcohols were partly dissolved in the aqueous phase and thus, not
270 detected in the separated non-aqueous phase in such high quantities. However, the
271 combined analysis of the aqueous and non-aqueous phase for the electrolysis with the
272 exemplary CA solution also showed smaller fractions of alcohols compared to case study A

(2.3% *vs.* 5.2%, Figure S4), indicating that less alcohols were formed in the exemplary CA mixture.

Note that also minor quantities of *n*-caprylic acid (0.4%) were detected in the harvested non-aqueous phase (Figure S4). Even though the majority of CA was present in the dissociated form during electrolysis, there was still a minor fraction of protonated CA that could have partitioned in the non-aqueous phase. This partitioning during the electrolysis was not detected for the electrolysis product analysis in case studies A and B, since the aqueous and non-aqueous phase were evaluated simultaneously and it was assumed that all CA detected were derived from the aqueous phase. The partitioning of the CA in the non-aqueous phase is not only a sink of CA, it also diminishes CA electrolysis product quality. Thus, highly alkaline pH values should be applied to minimize the risk of CA getting extracted by the non-aqueous electrolysis product phase.

S 2.4 Step 3 – *Kolbe electrolysis:* Oxygen, hydrogen and carbon content of non-aqueous, liquid electrolysis product

The oxygen, hydrogen and carbon contents by weight of the CA electrolysis product given in Table 5 (see article) were derived from GC-MS data. Though the oxygen content of the electrolysis product (0.7%, *i.e.* <1%) was below the maximum for gasoline[4], the electrolysis step has to be designed carefully to minimize the fraction of alcohols, acids and esters in the non-aqueous electrolysis product. Besides preferring MCCA over short-chain CA, the bulk pH should be fairly alkaline to avoid partitioning of the strongly hydrophobic CA in the non-aqueous electrolysis product phase. Whereas the carbon content of the electrolysis product was slightly below the suggested range for diesel (84.1 wt% *vs.* 86.2 wt%), the hydrogen content was higher than allowed by the legal recommendations in Germany (15.1 wt% *vs.* 13.5 wt%)[5]. For one, this discrepancy is observed due to the different chain lengths of *n*-alkanes, being in the range of 10 to 25 C-atoms for diesel, but in the range of 7 to 15 C-atoms for the electrolysis product from MCCA with 6 to 8 C-atoms[5]. Yet, the major reason for exceeding the hydrogen content is that diesel (and gasoline, respectively) contain aromatic compounds with higher carbon-to-hydrogen ratios (*e.g.* benzene C_6H_6 *vs.* hexane, C_6H_{14}), whereas the electrolysis product is free of aromatic compounds (Table 5). Consequently, the electrolysis product also exceeds the recommendations regarding the *n*-alkane and *n*-alkene content by far (Table 5). Whereas high amounts of *n*-alkanes are desirable for diesel to improve ignition properties, gasoline requires the opposite to retain a high resistance towards self-ignition (knock resistance)[6].

S 2.5 Estimation of temperature dependent density

The density, ρ, of the non-aqueous electrolysis product (0.75 $\pm$ 0.01 g mL^{-1} at 22°C) was determined at room temperature (22°C, details see section S 3.3). In order to compare ρ of the electrolysis product to the recommendations for gasoline and fuel at 15°C, it was therefore necessary to convert the measured ρ to lower temperatures. The ρ conversion performed in this study was based on assumptions that are detailed in the following.

In eq. S13, the temperature dependent ρ of various organic compounds is described with T in K and ρ in kmol m^{-3}. The respective compound-specific constants B_1, B_2, B_3 and B_4 can be reviewed in charts[7].

$$\rho\,(T) = \left(\frac{B_1}{B_2}\right)^{\left[1+\left(1-\frac{T}{B_3}\right)^{B_4}\right]} \qquad \text{(eq. S13)}$$

Since *n*-alkanes with 7 to 14 C-atoms and 1-heptene were found to be the main component of the liquid electrolysis product (Figure S4), we calculated the density increase for each of these compounds for the temperature difference between 25°C and 15°C. However, using the molar mass of each compound and the respective conversing factor for the volume, ρ can be expressed in g cm^{-3}.

Table S4 lists the factors B_1 to B_4 and the derived ρ for each compound at 15°C and at 25°C. The average increase of ρ for a temperature decrease from 25°C to 15°C for all the mentioned main electrolysis products components was observed to be 1%. Consequently, the ρ of the electrolysis product was converted by increasing the measured ρ value at 22°C by 1% to be valid at 15°C, *i.e.* 0.76 $\pm$ 0.01 g mL^{-1}.

Table S 4: Constants for temperature dependent density of main components of the liquid electrolysis product[7].

Component	Molar mass [g mol^{-1}]	B_1[7]	B_2[7]	B_3[7]	B_4[7]	ρ (15°C) [g cm^{-3}]	ρ (25°C) [g cm^{-3}]	ρ (25°C) / ρ (15°C)
n-heptane	100.20	0.612590	0.26211	540.20	0.28141	0.690	0.682	101.2%
n-octane	114.20	0.537310	0.26115	568.70	0.28034	0.707	0.699	101.1%
n-nonane	128.30	0.483870	0.26147	594.60	0.28281	0.722	0.715	101.0%
n-decane	142.30	0.428310	0.25745	617.70	0.28912	0.734	0.727	101.0%
n-undecane	156.30	0.390000	0.25678	639.00	0.29130	0.744	0.736	101.0%
n-dodecane	170.30	0.355441	0.25511	658.00	0.29368	0.752	0.745	100.9%
n-tridecane	184.39	0.321600	0.25040	675.00	0.30710	0.761	0.754	100.9%
n-tetradecane	198.39	0.305450	0.25350	693.00	0.30538	0.766	0.759	100.9%
1-heptene	98.19	0.637340	0.26319	537.29	0.27375	0.701	0.693	101.2%
average								**101.0%**

S 2.6 Brief comparison to established biofuels

As discussed in the main article, the product is considered as a renewable suitable fuel-additive, similarly to HVO and FAME. First of all, the gained product possesses a similar composition (Figure S4) as HVO, which contains mainly *n*-alkanes and *iso*-alkanes[5,6]. The main differences in the composition are the lack of *iso*-alkanes and the occurrence of minor quantities of oxygen containing carbon compounds (Figure S4) in the product. But since the oxygen content of the electrolysis product was <1% (Table 5), it is speculated that its addition yields a positive effect on the diesel fuel performance similar to adding HVO. For instance, adding HVO to diesel increases the cetane number (min. 51)[8], and thus improves ignition properties[5,6]. Further, CO emissions are reduced and the amount of unburned hydrocarbons (soot formation) is decreased when HVO is added to diesel[5,6]. Yet, HVO is produced from biological triglycerides by applying high temperatures and hydrogen pressures, which is potentially more energy intense then the microbial and electrochemical conversion [5,6]. Thus, compared to HVO production, the electrolysis product might be accessible with lower energy expenditure, as neither high temperatures nor elaborated hydrogen pressures are required. In addition to HVO, fatty acid methyl esters (FAME) are also extensively used as diesel additives, and therefore FAME are potentially competing with the diesel fuel additive produced in this study. However, due to the excellent stability and the low polarity of the *n*-alkanes being the main products of the electrolysis, we speculate that the electrolysis product has superior properties compared to FAME[9]. Additionally, the proposed process applies carbohydrate-rich substrates (*e.g.* crops) in contrast to HVO and FAME, whose production is based on fats (*e.g.* waste oil or plant oil). Moreover, in line with the biorefinery concept, whole plants can be exploited in the proposed process, by exploiting fermentation residues for biogas production, which we consider as an additional advantage over conventional bio-based fuel additives.

S 2.7 Overall performance and engineering of the process-line

Generally, the CA derived from pre-fermented (corn-based) model substrates were successfully and reproducibly converted to a variety of organic products which could be applied as a drop-in fuel respectively fuel additive in the discussion if the main article. For case study A, liquid hydrocarbons dominated the product spectrum, whereas shorter, more volatile hydrocarbons and alcohols were the main CA electrolysis products in case study B (Figure 2). Note that the reported yields for the final products reported in Table 2 are slightly underestimated due to the incomplete recovery of converted CA in identified products as discussed. However, on a technical scale (*i.e.* in a stainless steel plant), the recovery of products can be expected to be much easier than on a labscale. The hydrocarbon yield obtained in case study A (0.480 g COD g^{-1} COD, Table 2) is highly remarkable, considering the conditions: anaerobic fermentation, complex substrates, and applying a reactor microbiome.

When comparing case studies A (using liquid feedstock) and B (using solid feedstock), we show that the optimum product spectrum is achieved when hydrophobic MCCA rather than short-chain CA are the main products of the fermentation (step 1, Figure 2 and Table 3). Thus, a crucial step is the adaptation of the reactor microbiome to produce the desired CA mixture, preferably MCCA. As the knowledge on MCCA fermentation rapidly increases[10] and it was recently shown that *n*-caprylic acid can be produced with 91-96% efficiency[1], we are confident that a selective CA fermentation can be achieved in future. Even *iso*-carboxylic acids, which could also be part of the CA spectrum[11,12] (as also observed in case study B, Table S3), can be decarboxylated electrochemically[13], and therefore valorized. However, an efficient and fast MCCA extraction system (*e.g*. pertraction) proved to be essential to stimulate anaerobic MCCA production. Fortunately, the MCCA extraction system as successfully established (*e.g.* by Agler *et al.*[14], Ge *et al.*[15], or Kucek *et at.*[16]) offers cheap operating costs and allows the recycling of the extraction solvent and phase transfer catalyst during a long period of time (four years of continuous CA extraction without performance loss of the recycled solvent). In addition, any NaOH that is added to maintain an alkaline pH in the back-extraction solution can also be recycled when the back-extraction solution is exchanged between extraction and electrolysis. Nevertheless, future studies are required to investigate the life-time of the membrane modules operated with complex substrates (*i.e.* diminish membrane fouling) and access the optimum volume scale proportions between bioreactor and back-extraction solution to enable a fast CA build-up *prior* to electrolysis. Here also other technologies like using decanters sieve belt presses, screw presses or filtration units may be considered.

The electrolysis of MCCA yielded excellent results in terms of *CE*, power input, and operating time (Table 4). Due to the phase separation of the aqueous reaction phase and the non-aqueous electrolysis product, only simple downstream processing is required to gain the final product (Figures 2 and S3). In addition to the liquid product, the gaseous and volatile products are easily captured. It is well known that introducing H_2 and CO_2 as main electrolysis exhaust gases to the anaerobic fermentation allows the fermentative production of ethanol, which in turn promotes CA chain elongation[10]. Therefore, future studies which recycle the electrolysis exhaust gases to the bioreactor might even further improve the overall process performance. This positive effect on the fermentation step is also expected when reintroducing the evaporated alcohols from the electrolysis to the fermentation broth[17].

Regarding the electrolysis step, the main challenge is the electrode engineering, as cheaper and more abundant materials than platinum as well as a 3D electrode architecture are needed to improve space-time yields. Alternative materials include non-noble metal alloys, glassy carbon, iridium and rhodium and alloys of rather low platinum loadings or boron-doped diamond electrodes[18–21]. Especially for large anodes, sputtering or vapor deposition on a backbone material may drastically reduce the amount of expensive metal catalyst required[22]. Applying sustainable and cost-competitive cathode materials for hydrogen evolution is also considered economically beneficial (*e.g.* molybdenum sulfides or transitions metals are promising candidates[23–25]). Fortunately, the alkaline pH of the back-extraction solution did not negatively affect the Kolbe electrolysis of sufficiently hydrophobic MCCA.

Overall, there are several critical aspects which may challenge the feasibility of the proposed future technology. For example, here we applied corn-based, that is food-competitive, model substrates to demonstrate the suitability of the proposed process concept. However, the proposed process allows recovering resources (MCCA and finally, hydrocarbons and other organic carbon compounds) from different biomass and waste streams[26]. For example, ethanol-rich substrates (*e.g.* residues form the bioethanol industry) showed the highest production rates of *n*-caproic acid by reactor microbiomes, so far[15,27]. Further, municipal solid wastes[28], lactate-rich substrates[29–31], wine lees[16], and wheat straw[32] are suited for CA production. Thus, treating waste streams from bioethanol industries or a combined processing of solid biomass and liquid waste streams seem to be the perfect setting. In addition to the biomass type, its local availability needs to be considered on a case-to-case basis.

S 3 Experimental

S 3.1 Step 1 – *Bioreactor*: Microbial carboxylic acid fermentation

Table S5 summarizes the characteristics of the liquid substrate that was fed to the anaerobic bioreactor for CA production in case study A and Table S6.

Table S 5: Corn kernel-to-ethanol fermentation beer (short: corn beer) composition per volume. The corn beer fed to the bioreactor in case study A was obtained from Western New York Energy in Medina, NY, USA. The presented data and standard deviation (SD) are based on n = 6 measurements.

Corn beer	pH	Ethanol [g L^{-1}]	Total solids [g TS L^{-1}]	Volatile solids [g VS L^{-1}]	Inert solids [g IS L^{-1}]	Total COD [g COD L^{-1}]	Soluble COD [g COD L^{-1}]
average	4.6	122.2	121.8	109.7	12.2	461.3 (460 for calculations)	350.4
SD	0.01	1.8	1.5	1.0	2.3	18.2	11.7

Table S 6: Composition of corn silage substrate applied in case study B. The corn silage fed to the batch bioreactor in case study B was obtained from a biogas plant in Neichen (Germany). The presented data and standard deviation (SD) are based on n = 2 (TS) or n = 3 (VS, IS) measurements.

Corn silage	pH	Total solids [g TS kg^{-1}]	Volatile solids [g VS kg^{-1}]	Inert solids [g IS kg^{-1}]	Total COD [g COD kg^{-1}]
average	3 to 4	348	337	11	337 (assumed according to [17,33])
SD	n.a.	n.a.	0.3	0.3	n.a.

S 3.2 Chemical Analysis

This study is an interdisciplinary work in which the experiments were carried out in three different labs. Thus, chemical analyses for the determination of concentrations were performed using different hardware. The following paragraph specifies the methodological details for each setup (*i.e.*, case study A or B, CA production and/or CA extraction, liquid and gaseous electrolysis product composition), also including protocols for the respective sample preparation (if required).

S 3.2.1 Analysis of carboxylic acids in aqueous solution

In case study A, the concentrations of CA in the bioreactor and the back-extraction solution were analyzed using gas chromatography as described previously[14].

In case study B, the concentrations of CA (acetic, propionic, *n*-butyric, *iso*-butyric, *n*-valeric, *iso*-valeric, *n*-caproic and *n*-caprylic acid) in liquid samples were determined in triplicate after derivatization using a 7890 A gas chromatograph (Agilent Technologies, Germany) equipped with a TurboMatrix 110 automatic headspace sampler (Perkin Elmer), an DB-FFAP column (0.5 µm × 250 µm × 60 m, Agilent Technologies) and a flame ionization detector. Nitrogen was the carrier gas with a flow rate of 3.62 mL min^{-1}. The chromatographic conditions were as follows: injector temperature, 220°C (split-splitless); detector temperature, 250°C; and an oven temperature program initiating at 40°C hold for 20 min followed by a temperature increase at a rate of 10 K min^{-1} up to 200°C. The supernatant of a centrifuged sample was diluted 1:5 (v:v) with deionized water and 3 mL were filled into a 20-mL glass vial. To each vial, 1 mL internal standard (2-methylbutyric acid), 0.5 mL methanol and 2.5 mL 1:5 (v:v) diluted sulfuric acid were added.

For off-line extraction of CA in case study B, the CA concentration in the process liquid and in the back-extraction solution was monitored using HPLC (Shimadzu Scientific Instruments). Compound identification and quantification was based on external standards (three point calibration, R^2 = 0.99). The analysis was performed with a refractive index detector (RID-10A) on a Hi-Plex H column (300 × 7.7 mm ID, 8 µm pore size, Agilent Technologies). The sample was injected at 50°C oven temperature and was eluted with 5 × 10^{-3} mol L^{-1} H_2SO_4 at 0.5 mL min^{-1}.

The concentration of CA prior and subsequent to electrolysis experiments (case study A, B and exemplary CA mixture) was monitored using the same HPLC system as described for the off-line extraction of CA in case study B, but was carried out at 65°C and was eluted with

5×10^{-3} mol L^{-1} H_2SO_4 at a flow rate of 0.6 mL min^{-1}. The HPLC data for CA in aqueous solution was used to calculate the CA consumption throughout the electrolysis. The aqueous sample for HPLC analysis was gathered by dipping a pipet tip in the aqueous/non-aqueous mixture after electrolysis (no removal of non-aqueous phase prior to HPLC sampling).

S 3.2.2 Analysis of liquid electrolysis product

The liquid electrolysis product of case study A or case study B was characterized using GC-MS analysis after the electrolysis was finished and a sample (200 µL) for HPLC analysis of the aqueous phase was gathered for quantifying CA consumption (details on HPLC analysis see above). The pH of the two-phase reaction volume (large amount of aqueous, small amount of non-aqueous phase, Figure S3) was adjusted to drop below pH 2 by adding 6 mol L^{-1} HCl. Due to acidification, most of the CA in the sample were protonated. Subsequently, *n*-pentane was used to extract the hydrophobic electrolysis products and the protonated CA to the non-aqueous phase (volume share *n*-pentane to electrolysis liquid equals 3 to 5, *i.e.* 30 mL *n*-pentane to 50 mL total electrolysis volume). Note that due to the extraction step in *n*-pentane, any *n*-pentane produced during electrolysis could not be detected. Other solvents for extraction *prior* to GC-MS analysis of the non-aqueous electrolysis products were also tested (*n*-hexane, dichlormethane, chloroform, methyl *tert*-butyl ether, ethyl acetate, diethyl ether, *iso*-octane and toluene), but *n*-pentane was suited best for liquid electrolysis product analysis *via* GC-MS despite the potential error of *n*-pentane loss.

The *n*-pentane phase enriched with electrolysis products was further diluted in *n*-pentane and analyzed via GC-MS (GC 7890A and MSD 5975 InertXL, Agilent), using a DB-FFAB capillary column (30 m, 0.25 mm, 0.25 µm, Agilent) with helium as carrier gas (nominal 1.2 mL min^{-1} constant flow, adjusted for retention time locking) and undecanoic acid methyl ester as internal control standard. The initial temperature was 50°C (hold for 2 min) and was increased to 250°C at a rate of 15 K min^{-1}.

CA, *n*-alkanes, alcohols and most of the expected esters were identified using retention times and mass spectra of pure compounds. Other products were identified by a mass spectrum database (NIST14 database). The concentrations of CA, *n*-alkanes and alcohols were determined using external standards and generation of a real-time calibration database (three calibration levels). The concentrations of esters and other products were estimated using an average response factor of all target compounds in the mentioned database.

Subsequent to the end of each electrolysis in case study B, the cooling trap was washed with 1 mL *n*-pentane. An aliquot was then injected to the GC-MS using the same settings as described above to determine the condensate composition. A second washing step with 1 mL fresh *n*-pentane was performed and the *n*-pentane of the second step was also analyzed. The concentration of the condensate found in step 1 and 2 of the washed cooling trap were summed up.

In some cases, the non-aqueous electrolysis product was harvested and separated from the aqueous phase after the electrolysis has finished (exemplary CA mixture used to collect larger amounts of non-aqueous product used for the comparison to fuel parameters). In this case, the extraction step was skipped and the non-aqueous sample was directly diluted in *n*-pentane. Besides that, the analytical workflow was identical to the workflow described above.

The water phase, depleted of electrolysis products due to *n*-pentane extraction, was diluted in acidic water (10×10^{-3} mol L^{-1} HCl) and analyzed via GC-MS using a ZB-WAXplus capillary column (30 m, 0.25 mm, 0.25 µm, Supelco) and propionic acid as internal control standard for samples derived from case study A (no internal control standard for case study B). Other GC-MS parameters and the identification/quantitation routine were the same as described for the non-aqueous phase.

S 3.2.3 Analysis of gaseous electrolysis product

In case study B, the exhaust gas of the electrolysis was collected in a gastight bag made of aluminum composite material (barrier material: Hermann Nawrot AG, Wipperfuerth, Germany). After the electrolysis, the total amount of exhaust gas was measured via water volume displacement, $V_{gas\_measured}$. The $V_{gas\_measured}$ was converted to the normal volume, V_0, with eq. S14 by considering the temperature, T, and pressure, p_L, of the environment (meteorological station (TFA 20.2027.20, TFA-Dostmann, Wertheim-Reicholzheim, Germany) in the lab) and assuming the vapor pressure of water for 100% water saturated air, p_W, in dependency of T and relate the value to the normal temperature, T_0 (273 K), and the normal pressure, p_0 (101.325 Pa). The composition of the exhaust gas was measured using a four channel (*i.e.* column) 3000 Micro GC Gas Analyzer (INFICON, Cologne, Germany) with a thermal conductivity detector (GC-TCD). For details on the configuration of the four columns, see Table S7. External standard calibration (at least two levels) enabled the determination of the molar fraction of hydrogen, oxygen, nitrogen, carbon dioxide, methane, ethane, ethene, propane, propene, *n*-pentane and *n*-hexane. Further, *n*-butane and 1-butene were detected as a joint peak.

$$V_0 = V_{gas\_measured} \cdot \frac{(p_L - p_W) \cdot T_0}{p_0 \cdot T} \qquad \text{(eq. S14)}$$

Subsequent to GC-TCD measurement, the absolute amount of each component in mol was calculated as described in DIN-14912, assuming that the gas mixture behaved like an ideal gas mixture of real gases. First, the average molar mass of the gas mixture was accessed by multiplying the molar fraction of each component by its particular molar mass and this was summed up over all identified components. Similarly, the mean volumetric density of the gas mixture was determined by multiplying the normal density of each component by its molar fraction and summing the factors up. For components that are not gaseous at normal conditions, the density at their boiling point, *i.e.* the lowest temperature at which the component is gaseous, was used instead of the density at normal state. Subsequently, the mass of the total gas mixture was calculated by multiplying V_0 with the average density of the gas mixture. In a next step, the mass of the gas mixture was divided by its mean molar mass, yielding the absolute amount of all gas particles in mol. Finally, the total amount of gas in mol was multiplied by the molar fraction of each gas to yield the absolute amount of each gas in mol.

Table S 7: Specification for exhaust gas composition analysis, *i.e.* gaseous electrolysis products, in case study B. All columns and injectors were provided by INFICON (Cologne, Germany).

Column/ Parameter	Unit	14 m Molsieve with 2 m Plot U pre-column, 1 µl backflush injector	8 m Plot Q, variable volume injector	8 m OV-1, 1.2 µm thick, variable volume injector	10 m Stabilwax, variable volume injector
carrier gas		argon	helium	helium	helium
sample inlet temperature	°C	100	100	100	100
injector temperature	°C	100	100	100	100
column temperature	°C	100	80	60	60
injection time	ms	0	25	250	250
running time	min	5	5	5	5
column pressure	psi	25	20	20	15

S 3.2.4 Analysis of the gas composition in the anaerobic fermentation

In case study A, the concentrations of methane, CO_2, and hydrogen gases were analyzed by gas chromatography as described earlier[16]. In case study B, one milliliter gas from the anaerobic fermentation process was injected into a 20 mL vial filled with argon. The samples were analyzed by gas chromatography (Clarus 580 with Turbomatrix™ Headspace Sampler 110, Perkin Elmer, Massachusetts, USA) using a thermal conductivity detector as well as two columns (7' HayeSep N 60/80, 1/8" Sf for analysis of CO_2 and 9' Molecular Sieve 13X 45/60 1/8" Sf for analysis of CH_4, H_2, O_2, and N_2). Argon was used as carrier gas at 25 mL min^{-1}. The temperatures of the injector, columns and detector were 150°C, 60°C and 200°C, respectively.

S 3.3 Characterizing fuel properties of the CA electrolysis product

The fuel characteristics of the liquid electrolysis product were accessed applying an exemplary CA solution, mirroring the composition of the main MCCA observed in case study A (Table S8). In total, the non-aqueous phase of 14 separate electrolysis of the exemplary CA mixture was merged, each of them yielding ≈2.5 mL liquid non-aqueous electrolysis product per 50 mL exemplary CA mixture (Figure S3). On average, 44% conversion of 0.97 mol L^{-1} CA (initial concentration, Table 3) were achieved. An aliquot of the merged non-aqueous, liquid electrolysis product of the exemplary CA mixture was used for characterizing selected fuel parameters, which are detailed below.

Table S 8: Composition of exemplary CA mixture applied for assessing fuel characteristics.

CA - name	**CA - composition [g L^{-1} / mol L^{-1}]**
n-caproic acid	39.0 / 0.33
n-enanthic acid	5.2 / 0.04
n-caprylic acid	86.2 / 0.60
sum	**130.4 / 0.97**

The composition of this accumulated electrolysis product was analyzed via GC-MS as described in S 3.2.2. The atom fractions of the electrolysis product (*i.e.* the carbon, hydrogen

and oxygen contents) were calculated based on the gravimetric concentration of each electrolysis product, the structural formula ($C_iH_jO_k$) and the particular molar mass.

The density of the liquid, non-aqueous electrolysis product was determined at room temperature (22°C) using a 5 mL pycnometer type Gay-Lussac (borosilicate glass 3.3, DIN ISO 3507, BRAND, Wertheim, Germany). The tare weight and the weight of the pycnometer filled with the aliquot of the sample were measured in three replicates.

The kinematic viscosity at 40°C was measured with a Stabinger viscometer (ASTM D445, SVM3000, Anton Paar GmbH, Graz, Austria, ASTM D445).

The water content was determined via coulometric Karl-Fischer-titration (DIN EN 14346, AQUA 40.00, ECH Elektrochemie Halle GmbH).

To characterize the energy content of the electrolysis product per mass, we determined the higher heating value (other names: gross calorific value or gross energy) at a constant volume by burning the electrolysis product in oxygen using a calorimetric bomb under the conditions specified in the standard operation procedure (DIN EN 14918, Parr 6400 Calorimeter, Parr Instrument (Deutschland) GmbH).

The analysis of sodium was performed by the ASG Analytik-Service Gesellschaft mbH (Neusäss, Germany) using a modified method according to the DIN-standard procedure for elemental analysis, especially determination of sodium, potassium, calcium, lead, nickel, phosphorous, copper and zinc contents in diesel fuel via inductively coupled plasma optical emission spectrometry (ICP-OES)[34].

S 4 References

1 L. A. Kucek, C. M. Spirito and L. T. Angenent, *Energy Environ. Sci.*, 2016, **9**, 3482–3494.

2 C. Stang and F. Harnisch, *ChemSusChem*, 2016, **9**, 50–60.

3 P. F. Levy, J. E. Sanderson, R. G. Kispert and D. L. Wise, *Enzyme Microb. Technol.*, 1981, **3**, 207–215.

4 DIN EN 228:2014-10, *DIN EN 228:2014-10 Kraftstoffe für Kraftfahrzeuge - unverbleite Ottokraftstoffe - Anforderungen und Prüfverfahren*, DIN-Normenausschuss Materialprüfung (NMP) Fachausschuss Mineralöl- und Brennstoffnormung (FAM), Berlin, 2012.

5 *Dieselkraftstoff - Anforderungen, Qualität, Perskeptiven*, Aral Aktiengesellschaft, Foschung und Technik, Bochum, 2010.

6 M. (Ed.) Lackner, F. Winter and A. K. Agarwal, *Handbook of combustion*, Wiley-VCH, Weinheim, 2010.

7 R. H. Perry, D. W. Green and J. O. Maloney, Eds., in *Perry's chemical Engineers' handbook*, The McGraw-Hill Companies, 7th edn., 1999, pp. 142–146.

8 *DIN EN 590:2014-04 Kraftstoffe für Kraftfahrzeuge - Dieselkraftstoff - Anforderungen und Prüfverfahren*, DIN-Normenausschuss Materialprüfung (NMP) Fachausschuss Mineralöl- und Brennstoffnormung (FAM), Berlin, 2014.

9 D. Yue, F. You and S. W. Snyder, *Comput. Chem. Eng.*, 2014, **66**, 36–56.

10 L. T. Angenent, H. Richter, W. Buckel, C. M. Spirito, K. J. Steinbusch, C. Plugge, D. P. B. T. B. Strik, T. I. M. Grootscholten, C. J. N. Buisman and H. V. M. Hamelers, *Environ. Sci. Technol.*, 2016, **50**, 2796–2810.

11 F. Morgan-Sagastume, S. Pratt, a Karlsson, D. Cirne, P. Lant and a Werker, *Bioresour. Technol.*, 2011, **102**, 3089–97.

12 P. J. Weimer, M. Nerdahl and D. J. Brandl, *Bioresour. Technol.*, 2015, **175**, 97–101.

13 A. J. Bard, M. Stratmann and H. J. Schäfer, *Encyclopedia of Electrochemistry: Volume 8: Organic electrochemistry*, Wiley-VCH Verlag, Weinheim, 2004.

14 M. T. Agler, C. M. Spirito, J. G. Usack, J. J. Werner and L. T. Angenent, *Energy Environ. Sci.*, 2012, **5**, 8189–8192.

15 S. Ge, J. G. Usack, C. M. Spirito and L. T. Angenent, *Environ. Sci. Technol.*, 2015, **49**, 8012–8021.

16 L. A. Kucek, J. Xu, M. Nguyen and L. T. Angenent, *Front. Microbiol.*, 2016, **7**, 1–14.

17 T. I. M. Grootscholten, F. Kinsky dal Borgo, H. V. M. Hamelers and C. J. N. Buisman, *Biomass and Bioenergy*, 2013, **48**, 10–16.

638 18 Y. B. Vassiliev and V. A. Grinberg, J*. Electroanal. Chem*., 1992, **336**, 281–307.

639 19 J. Barroso, a. R. Pierna, T. C. Blanco, E. Morallón and F. Huerta, *Int. J. Hydrogen*
640 *Energy*, 2011, **36**, 12574–12582.

641 20 A. Kapałka, B. Lanova, H. Baltruschat, G. Fóti and C. Comninellis, *J. Electrochem. Soc*.,
642 2008, **155**, E96.

643 21 J. D. Wadhawan, F. J. Del Campo, R. G. Compton, J. S. Foord, F. Marken, S. D. Bull, S.
644 G. Davies, D. J. Walton and S. Ryley, *J. Electroanal. Chem*., 2001, **507**, 135–143.

645 22 H. J. Schäfer, in *Topics in Current Chemistry, Vol. 152, Electrochemistry IV*, ed. E.
646 Steckhan, Springer, Berlin, Heidelberg, 1990, pp. 91–151.

647 23 D. Merki and X. Hu, *Energy Environ. Sci*., 2011, **4**, 3878.

648 24 D. Kong, J. J. Cha, H. Wang, H. R. Lee and Y. Cui, *Energy Environ. Sci*., 2013, **6**, 3553.

649 25 B. Konkena, K. junge Puring, I. Sinev, S. Piontek, O. Khavryuchenko, J. P. Dürholt, R.
650 Schmid, H. Tüysüz, M. Muhler, W. Schuhmann and U.-P. Apfel, *Nat. Commun*., 2016, **7**,
651 12269.

652 26 C. M. Spirito, H. Richter, K. Rabaey, A. J. M. Stams and L. T. Angenent, *Curr. Opin.*
653 *Biotechnol.*, 2014, **27**, 115–22.

654 27 D. Vasudevan, H. Richter and L. T. Angenent, *Bioresour. Technol*., 2014, **151**, 378–82.

655 28 T. I. M. Grootscholten, D. P. B. T. B. Strik, K. J. J. Steinbusch, C. J. N. Buisman and H.
656 V. M. Hamelers, *Appl. Energy*, 2014, **116**, 223–229.

657 29 H. Sträuber, M. Schröder and S. Kleinsteuber, *Energy. Sustain. Soc*., 2012, **2**, 13.

658 30 H. Sträuber, R. Lucas and S. Kleinsteuber, *Appl. Microbiol. Biotechnol*., 2016, **100**, 479–
659 491.

660 31 L. A. Kucek, M. Nguyen and L. T. Angenent, *Water Res*., 2016, **93**, 163–171.

661 32 H. Sträuber, F. Bühligen, S. Kleinsteuber, M. Nikolausz and K. Porsch, *Bioengineering*,
662 2015, **2**, 66–93.

663 33 E. ten Brummeler, PhD Thesis *Dry Anaerobic Digestion of the Organic Fraction of*
664 *Municipal Solid Waste,* Wageningen University, 1993.

665 34 *DIN EN 16476:2014-07 Flüssige Mineralölerzeugnisse - Bestimmung des Gehalts an*
666 *Natrium, Kalium, Calcium, Phosphor, Kupfer, Zink in Dieselkraftstoffen - Direkte*
667 *Bestimmung durch optische Emissionsspektrometrie mit induktiv gekoppeltem Plasma*
668 *(ICP OES)*, DIN-Normenausschuss Materialprüfung (NMP) Fachausschuss Mineralöl-
669 und Brennstoffnormung (FAM), Berlin, 2014.